Mapping the absolute electromagnetic field strength of individual field components inside a photonic crystal

T. Denis[a], B. Reijnders[a], J. H. H. Lee[a], W. L. Vos[b], K.-J. Boller[a], and P. J. M. van der Slot[a]

[a]Laser Physics and Nonlinear Optics, MESA+ Institute for Nanotechnology, University of Twente, P.O.Box 217, 7500 AE Enschede, The Netherlands

[b]Complex Photonic Systems (COPS), MESA+ Institute for Nanotechnology, University of Twente, P.O.Box 217, 7500 AE Enschede, The Netherlands

ABSTRACT

We present a method to map the absolute electromagnetic field strength inside photonic crystals. We demonstrate our method by applying it to map the electric field component E_z of a two-dimensional photonic crystal slab at microwave frequencies. The slab is placed between two mirrors to create a resonator and a subwavelength spherical scatterer is scanned inside the resonator. The resonant Bloch frequencies shift depending on the electric field at the scatterer position. By measuring the frequency shift in the reflection and transmission spectrum versus the scatterer position we determine the field strength. Excellent agreement is found between measurements and calculations without any adjustable parameters and a possible realization is suggested for measurements at optical frequencies.

Keywords: photonic crystals; photonic bandgap materials; nanophotonics; electromagnetic field measurement; near-field scanning optical microscopy

1. INTRODUCTION

Photonic crystals, structures in which the dielectric constant varies periodically on the order of the wavelength,[1] are frequently studied today as they offer a remarkable control over the emission of light.[2] This most intriguing capability of photonic crystals arises because photonic crystals shape the local density of electromagnetic states (LDOS).[3] Such control provided by photonic crystals has for example been demonstrated to enhance or inhibit the spontaneous emission from quantum dots,[4–9] which forms the basis for investigating the strong-coupling cavity regime in quantum electrodynamics.[10] Further, photonic crystals also have far reaching technological impact on, for example, the development of efficient micro-scale lasers, LEDs or solar cells.[11–18]

The LDOS depends on the electromagnetic field strength of the various Bloch modes inside the photonic crystal at the location of each individual emitter.[3] For ideal photonic crystals, *i.e.*, crystals with a perfect periodicity, the Bloch modes can be calculated by numerical methods. Examples are eigenmode or finite-difference time-domain (FDTD) techniques.[19–22] However, real photonic crystals unavoidably suffer from unpredictable non-periodic local deviations, *e.g.*, due to fabrication errors. Such deviations are very challenging to include into numerical calculations and can effectively not be modeled, even when most sophisticated methods are used.[23,24] A direct measurement of the electromagnetic fields inside the real photonic crystal is therefore desirable.

To date the most commonly used technique for mapping the electromagnetic field of Bloch modes is near-field scanning optical microscopy.[25–43] However, this technique is restricted to probe local fields *outside* the crystal near its surface while the field deep *inside* the crystal cannot directly be mapped. To get any estimate of the internal field strength one needs to make assumptions about the scattering for the internal fields under study to the detected external fields, which is extremely difficult.[33] Therefore, it is desirable to devise an alternative method that can probe the strength of the electromagnetic field *inside* a photonic crystal. For a complete characterization of the LDOS this field measurement method should be capable to resolve the direction and

Further author information: (Send correspondence to P. J. M. van der Slot)
P. J. M. van der Slot: E-mail: p.j.m.vanderslot@utwente.nl, Telephone: +31 (0)53 489 3967

Photonic and Phononic Properties of Engineered Nanostructures III,
edited by Ali Adibi, Shawn-Yu Lin, Axel Scherer, Proc. of SPIE Vol. 8632, 863211

· doi: 10.1117/12.2002945

absolute value of all individual field components (E_x, E_y, E_z, H_x, H_y, H_z). Such measurement method that determines the absolute electromagnetic field strength *inside* a real photonic crystal has never been reported.

Here we demonstrate a method to measure the absolute strength of the electromagnetic field distribution *inside* photonic crystals. Our method relies on measuring the resonant frequencies of standing waves in a photonic crystal of finite length that is enclosed by two mirrors.[44] A subwavelength scatterer placed inside the crystal scatters the electromagnetic field. The leads to a shift of the resonant frequency of the Bloch modes proportionally to the square of the electric and magnetic field strength at the scatterer position.[45–48] To map the field strength versus position, we measure the frequency shift as a function of the spatial position of the scatterer. By demonstrating the method at microwave frequencies we can limit fabrication errors to small values. Furthermore, the typical feature sizes of microwave photonic crystals are sufficiently large, meaning that a scatterer can be conveniently scanned through the crystal. To simplify the demonstration we deliberately choose a photonic crystal design where a single field component inside the microwave photonic crystal slab dominates throughout most of the crystal. Using a spherical, metallic bead as a scatterer we can then map the dominant electric field component E_z *inside* a photonic crystal slab.

2. MEASUREMENT METHOD

To map the electromagnetic field, the photonic crystal is sandwiched between two mirrors. The mirrors enforce that the electromagnetic field in the photonic crystal can only build up at discrete resonance frequencies ν_0. The associated electromagnetic field distribution at such frequencies will be denoted as longitudinal modes in the following. To measure the electromagnetic field we place a scatterer inside the photonic crystal and measure the induced frequency shift of the longitudinal modes $\Delta\nu$. We chose a scatterer in the Rayleigh regime. This means that the size parameter of the scatterer is $x \ll 1$, with $x = 2\pi R/\lambda$. Here, R is the radius of the object and λ the wavelength. In the Rayleigh regime the field is approximately constant throughout the scatterer volume. In this case the scattering can be described by the electrostatic approximation to calculate the resulting frequency shift $\Delta\nu$ due to the scatterer. Using a spherical metallic scatterer with a radius R we obtain[45–47]

$$\Delta\nu(\mathbf{r}) = \frac{\frac{1}{2}\mu_0\mathbf{H}(\mathbf{r})^2 - \epsilon_0\mathbf{E}(\mathbf{r})^2}{U}\pi R^3\nu_0. \tag{1}$$

Here $\mathbf{E}(\mathbf{r})$ and $\mathbf{H}(\mathbf{r})$ are the unperturbed electric and magnetic fields at the location $\mathbf{r}$ of the scatterer, respectively. U is the total energy stored inside the unperturbed photonic crystal cavity, ϵ_0 is the permittivity and μ_0 the permeability of free space. By measuring the frequency shift $\Delta\nu$ versus the scatterer location $\mathbf{r}$ we can map, in a general photonic crystal, the electromagnetic field quantity $\left(\frac{1}{2}\mu_0\mathbf{H}(\mathbf{r})^2 - \epsilon_0\mathbf{E}(\mathbf{r})^2\right)$. In certain photonic crystal geometries particular field components dominate, *i.e.*, the field strength of a single component can be much greater than for all other components. Measuring the total field is then effectively a measurement of this dominating field component.

For example, if the longitudinal electric field component dominates above all other field components the frequency shift becomes

$$\Delta\nu(\mathbf{r}) \approx -\frac{\epsilon_0 E_z(\mathbf{r})^2}{U}\pi R^3\nu_0 \tag{2}$$

Solving for the E_z component yields

$$E_z(\mathbf{r}) = \sqrt{\frac{-\Delta\nu(\mathbf{r})U}{\pi R^3\epsilon_0\nu_0}}. \tag{3}$$

Equation (3) illustrates how to map the absolute strength of the E_z field component. By measuring the frequency shift of the longitudinal resonances versus the bead position *inside* the crystal we retrieve the absolute strength of the electric field component E_z at that location. Note that in order to measure the absolute field strength we have to know the stored energy U inside the photonic crystal cavity for a given input power P_{in}. This can be separately determined by measuring the quality factor of the resonator at the considered resonant frequency.

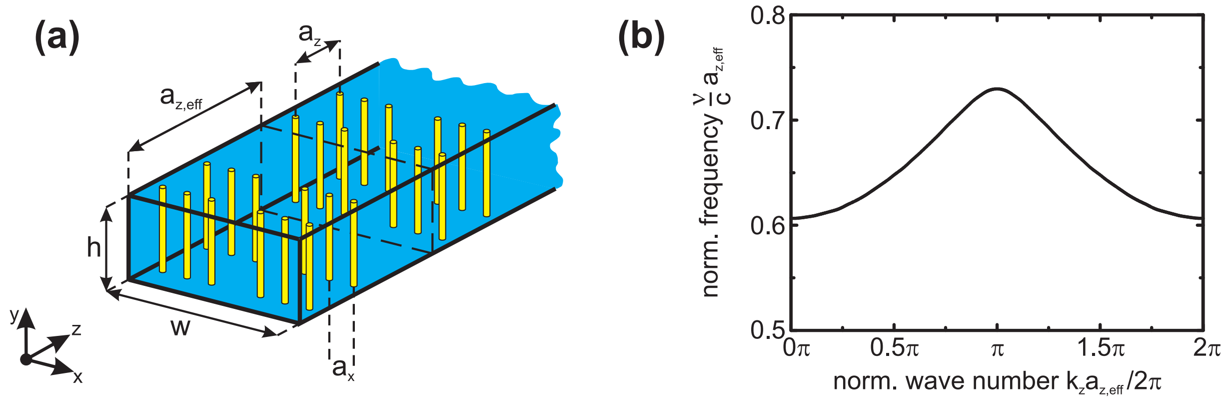

Figure 1. (a) Schematic three-dimensional view of the photonic crystal slab. Metallic rods are placed inside a rectangular metallic waveguide. The dashed line shows the size of the supercell. (b) Calculated band structure of the photonic crystal slab showing the lowest-frequency Bloch mode having a dominating E_z component of the electric field.

3. PHOTONIC CRYSTAL SLAB

For the demonstration of the field mapping method we choose a particular crystal geometry with a dominating E_z field component, which properties we present in this section. Figure 1a shows the unit cell of the photonic crystal slab. A rectangular lattice of metal rods is enclosed inside a rectangular metal waveguide causing the E_z field component to dominate above all other field components inside the structure for a certain set of Bloch modes. The photonic crystal has a lattice constant of $a_z = 7.5\,\text{mm}$ along the z-direction and the lattice constant is $a_x = 6.75\,\text{mm}$ along the x-direction. However, the unit cell is a supercell geometry, motivated by the intended application of the slab in a photonic free-electron laser.[49] The supercell contains a central line defect at $x = 0$ and each third transverse row of rods is missing. In total the supercell consists of 12 rods and has a length of $a_{z,\text{eff}} = 22.5\,\text{mm}$, as indicated in Fig. 1a. The diameter of the rods is 4 mm and the surrounding waveguide has a width of $w = 47.25\,\text{mm}$ and a height of $h = 20\,\text{mm}$.

The band structure of this photonic crystal slab is calculated via a FDTD method.[22] For these computations, periodic boundary conditions are applied to the unit cell along the z-direction. Accordingly, the photonic crystal slab is modeled to be infinitely long in the z-direction. For simplicity, the metallic parts of the slab are assumed to be perfect electric conductors which is well justified in the microwave range. Figure 1b shows the results for the lowest-frequency Bloch mode with a dominating longitudinal electric field component. We depict only the dispersion in the first Brillouin zone ($0 < k_z a_{z,\text{eff}} < 2\pi$), where k_z is the wave number. Due to the periodicity the dispersion repeats for frequencies outside the first Brillouin zone. Furthermore, the finite transverse size of the waveguide results in a lowest allowed normalized frequency of $\nu a_{z,\text{eff}}/c = 0.61$ for the specific mode under investigation.

For a comparison with experimental field mapping data we calculate the local E_z field distribution of the Bloch mode. The FDTD method is applied for a normalized wave number of $a_{z,\text{eff}}\, k_z = 0$ which corresponds to a normalized frequency of 0.61. Figure 2 shows the E_z field pattern of the mode at the transverse plane at $z = 2.5a_z$ where mapping will be performed. The strongest field strength of the E_z component is found near the waveguide center ($x = 0$, $y = 0$). Further, due to the boundary conditions, the E_z field component approaches zero at the inner surface of the waveguide, as expected for the electric field tangential to a perfect electric conductor.

4. EXPERIMENTAL SETUP

A schematic view of the experimental setup is shown in Fig. 3a. A resonator is formed via placing two highly reflective aluminum mirrors around the high-precision manufactured photonic crystal, whose properties have been described in section 3. In the longitudinal direction, the resonator contains a total of 15 supercells. The first mirror is positioned at a distance of $0.5a_z$ from the center of the first row of rods and the second mirror is positioned at a distance of $1.5a_z$ from the last row of rods.

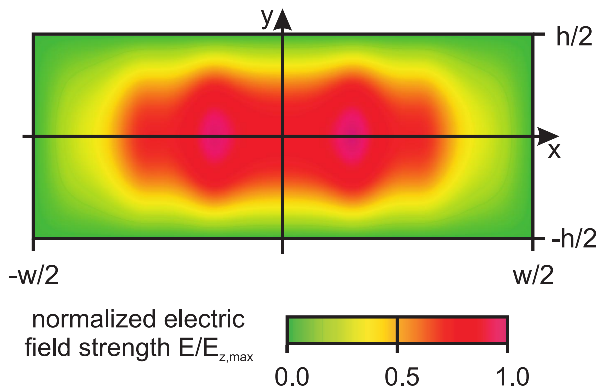

Figure 2. Transverse longitudinal electric field distribution, E_z, of the photonic crystal slab for the investigated mode at a cross sections $z = 2.5a_z$ inside the unit cell. The normalized wave number is $k_z a_{z,\mathrm{eff}} = 0$ and the corresponding normalized frequency is 0.61.

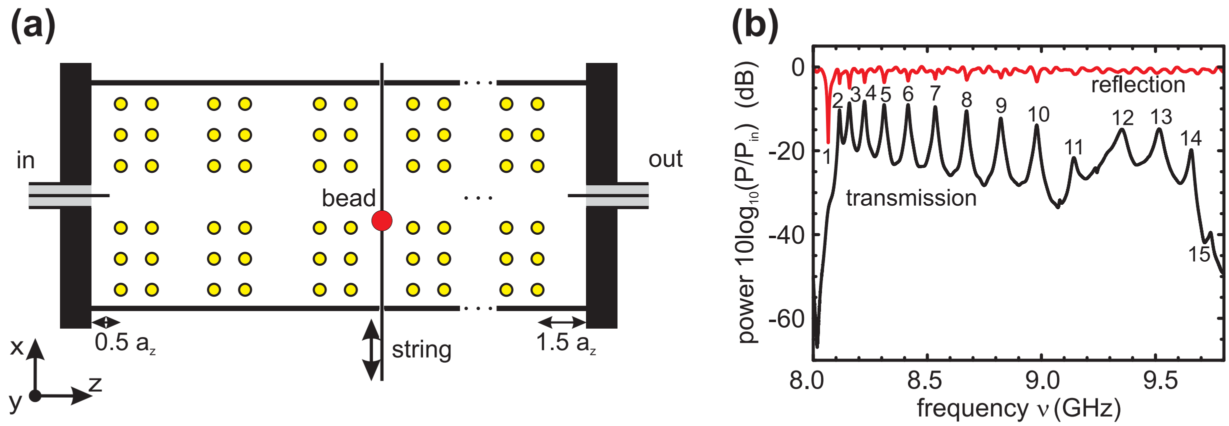

Figure 3. (a) Top view of the experimental setup for electromagnetic field mapping inside the photonic crystal slab. The figure shows a cross section through the photonic crystal slab at $y = 0$. The photonic crystal slab is sandwiched between two aluminum mirrors (bold black). The input and output antennas are mounted at the center of both mirrors. To map the E_z field component along the x-direction a spherical metallic scatterer, which is mounted on a string, can be moved throughout the photonic crystal slab. (b) Transmission and reflection spectrum of the photonic crystal slab without a scatterer between 8.0 GHz and 9.8 GHz.

To fabricate the photonic crystal slab the following steps are performed. A channel with a rectangular cross section of $47.25\,\mathrm{mm} \times 20\,\mathrm{mm}$ is milled into a solid aluminum block (bottom plate) and is covered with an aluminum top plate. Both plates contain holes for mounting the rods. The rods are hollow brass cylinders with an inner diameter of 2 mm and an outer diameter of 4 mm. The rods are positioned with screws extending from the top plate through the rods and attach into the bottom plate. At the same time this secures a good electrical connection between the rods and the waveguide. The total positioning accuracy for the rods is estimated to be less than $100\,\mu$m or 1.4% of the inter rod distances.

To measure the resonant frequencies of the photonic crystal slab cavity, an antenna[50] is mounted at the center of each mirror (see Fig. 3). One antenna acts as an emitter while the other antenna acts as a receiver. To find a good compromise between minimal loading of the resonator by the antennae and sufficiently high coupling to the mode, the length of both antennas was about 4 mm. The other end of both antennae is connected to a network analyzer via coaxial SMA cables. The network analyzer is formed using a tunable microwave source with a maximum frequency of 20 GHz (Wiltron, model 69147A), two directional couplers (Krytar, model 2610) and two microwave power meters (Anritsu, model ML1438A with power heads MA2444A and MA2424B). The network analyzer is calibrated before the measurements to compensate for losses in its components. The accuracy is estimated to be about 10%. This setup allows measuring the reflection and transmission spectra of the photonic crystal slab cavity. For the measurements a frequency resolution of 250 kHz is used and the input power P_{in} from the network analyzer is 1 mW.

To map the electromagnetic field inside the photonic crystal slab the scatterer is scanned through the inside of the photonic crystal. The scatterer is a stainless steel bead with a radius of $R = 2$ mm. The bead is mounted on a 0.3 mm thick nylon string. As shown in Fig. 3a the string runs through two small holes (300 μm) in the opposing side walls. One end of the string is mounted on a translation stage and the other end of the string is attached to a weight to keep the string straight via tension. The translation stage positions the bead with a relative accuracy of better than 0.05 mm and a absolute accuracy of better than 0.1 mm.

5. DISPERSION MEASUREMENT

Before measuring the E_z-field component of the photonic crystal slab resonator we verified the appropriate description of the slab using the FDTD model. Specifically, to confirm the crystal dispersion, we measured the resonance frequencies of the different longitudinal and transverse modes without a scatterer inside the photonic crystal. Measuring the dispersion is based on determining the longitudinal resonance frequencies of a finite-length photonic crystal consisting of n unit cells and assigning wave numbers to each observed resonance frequency.[51] For the assignment we consider the phase advance $\delta\phi$ of the field per round trip in the resonator. At each longitudinal resonance the phase advance per round trip along the z-direction is a multiple of π:

$$\delta\phi = na_{z,\text{eff}}\, k_z = m\pi \qquad\qquad m = 1, 2... \tag{4}$$

Here $na_{z,\text{eff}}$ is the geometrical length of the resonator and k_z is the wave number in the first Brillouin zone. As the resonator mirrors enclose $n = 15$ unit cells of the photonic crystal, 15 longitudinal resonances with a finite wavelength are expected[51] having a normalized wave number $a_{z,\text{eff}}\, k_z$ of

$$0 < a_{z,\text{eff}}\, k_z = \frac{m}{n}\pi \leq \pi. \tag{5}$$

From the dispersion shown in Fig. 1b the frequency of mode is seen to be a monotonously increasing function of the wave number in the first half of the Brillouin zone. This renders the resonances denumerable. By using eq. (5), a normalized wave number can be associated to each longitudinal resonance frequency, from which the dispersion of the studied mode is obtained.

Figure 3b shows the measured transmission and reflection power spectrum of the unperturbed photonic crystal slab resonator in the range from 8 GHz to 9.8 GHz on a logarithmic power scale. For most of the measured frequencies the reflection is close to 0 dB meaning that it is equal to the input power of 1 mW. Due to the resonator an electromagnetic field can only build up at frequencies where longitudinal resonances of a transverse photonic crystal mode exist. In both spectra we clearly observe resonances which we assign to the various longitudinal modes. As expected for such resonances the frequency of reflection and transmission resonances agree very well with each other. For our photonic crystal slab of 15 unit cells, we expect from theory to observe 15 longitudinal resonances with a finite wavelength belonging to mode 1 and indeed, inspecting the transmission and reflection spectra, 15 resonances are observed. The first resonance is only clearly visible in the reflection spectrum. Furthermore, the resonances above the tenth one are only visible in the transmission spectrum. The signal-to-noise ratio is too low to detect all resonances in the reflected signal. When using these considerations, eq. (5) can be used to assign wave numbers to each measured resonance frequency of the mode, as plotted in Fig. 4a. We find an excellent agreement between the experimentally determined data points and the numerically calculated dispersion (solid line). This excellent agreement indicates an appropriate description of the fabricated slab with FDTD calculations.

6. ELECTRIC FIELD MEASUREMENTS

We map the longitudinal electric field inside the photonic crystal slab by measuring the frequency shift of an individual longitudinal resonance as a function of the scatterer position. Note that the measured frequency shift $\Delta\nu$ is referenced to the resonance frequency of the resonator loaded by the nylon string alone. The effect of the nylon string is small as it results in a shift of only 250 kHz.

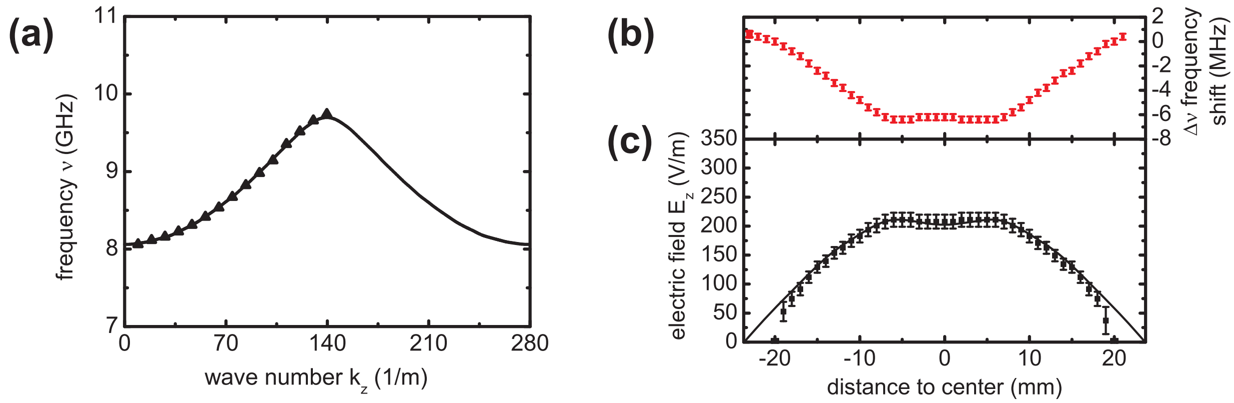

Figure 4. (a) Measured dispersion of the photonic crystal slab (symbols) compared to the calculated values from Fig. 1b (b) Measured frequency shift $\Delta\nu$ induced by the spherical scatterer placed at that location. Shown is the frequency shift $\Delta\nu$ for the longitudinal mode with $\nu = 8.22\,\text{GHz}$ and $k_z a_{z,\text{eff}} = \frac{4}{15}\pi$. (c) Resulting electric field component E_z from the measured frequency shift shown in (b). The measured electric field component E_z (symbols) is compared to the calculated electric field (lines).

Figure 4b shows an example of the measured frequency shift $\Delta\nu$ for the longitudinal mode with a frequency of $\nu = 8.22\,\text{GHz}$ corresponding to a normalized wavenumber of $k_z a_{z,\text{eff}} = \frac{4}{15}\pi$. The uncertainty in the frequency shift is 250 kHz due to the chosen frequency resolution of the network analyzer. Throughout the measurements the frequency shift is mostly much smaller than zero indicating that the contribution from the electric field components indeed dominates above magnetic field components. Towards the edge of the waveguide the frequency shift $\Delta\nu$ approaches zero, as expected from the electric field computed from the numerical calculations (see Fig. 2). The highest absolute value in frequency shift of about 5.2 MHz is found 5.0 mm away from the center. Indeed, also the numerical calculation of the electric field predict that the E_z field component has its maximum strength along the x-direction slightly off the waveguide center (see Fig. 2).

To calculate the longitudinal electric field E_z from the measured frequency shift we apply eq. (3). However, this requires to determine the total energy stored inside the cavity U. To retrieve U we use the definition of the quality factor:

$$Q = 2\pi\nu_0 \frac{U}{P_{diss}}. \tag{6}$$

Exactly at resonance the dissipated power per cycle P_{diss} is equal to the input power P_{in} from the network analyzer. To retrieve the experimental Q-values we determine the full width half maximum of each transmission resonance ν_{FWHM} shown in Fig. 3b and use $Q = \nu_0/\nu_{\text{FWHM}}$.

Figure 4c shows the resulting electric field strength E_z (square dots) determined from the found frequency shift. For a comparison, the figure displays also the calculated E_z field strength at these positions determined by the FDTD computations presented in section 3 (black line). Uncertainties for the measured field values are determined by using the Gaussian error propagation law. We assume that the dominating errors are the uncertainty in input power of about 10 % and the frequency resolution of 250 kHz. Other uncertainties are neglected as these are much smaller and accordingly do not significantly contribute to the error in the measurement.

7. CONCLUSION

We have demonstrated for the first time a method for mapping the absolute strength of an electromagnetic field component *inside* a photonic crystal. The method relies on measuring the change in resonance frequency when the photonic crystal is placed inside a resonator and the field inside the photonic crystal is perturbed by a sub-wavelength scatterer. A spherical scatterer is applied to measure the dominating longitudinal electric field E_z in a specific photonic crystal slab. We observe a good agreement between measured and calculated electric field strength E_z without using any adjustable parameters in the calculations. Note that even if all six components would be of comparable strength, such as in an arbitrary photonic crystal or at specific locations, it is still possible to separately measure each field component. This can be achieved by selecting for the scatterer a suitable material, shape and orientation such that only a single field component contributes to the frequency shift.[45,46] For example, a thin metallic needle would short-circuit and thus probe the electric field along the orientation of the needle while leaving all other field components unaffected.

In the future, this method could be applied in the near infrared or optical domain by scaling down the photonic crystal and the bead on a string. To induce a space dependent frequency shift a metallic or dielectric scatterer could be placed on a carbon nanotube acting as a string. To control the nanotube it could be attached to an atomic force microscope tip. Mounting a carbon nanotube on an atomic force microscope has been demonstrated.[52] Further, atomic force microscopy allows a sufficiently high spatial resolution, demonstrated by recent measurements where an emitter directly mounted to an atomic force microscope has been used to map the emitter lifetime around a single nanorod.[53] By combining these results it should be possible to measure the shift in resonance frequency in the transmission spectrum to determine the absolute field strength inside the air voids of a photonic crystal at optical frequencies.

ACKNOWLEDGEMENTS

This research is supported by the Dutch Technology Foundation STW, applied science division of NWO and the Technology Program of the Ministry of Economic Affairs. The authors further thank ESA-ESTEC for providing part of the RF-equipment. The research is also part of the strategic research orientation Applied Nanophotonics within the MESA+ Research Institute.

REFERENCES

[1] Joannopoulos, J. D., Johnson, S. G., Winn, J. N., and Meade, R. D., [*Photonic crystals: molding the flow of light*], Princeton University Press (2008).

[2] Yablonovitch, E., "Inhibited spontaneous emission in solid-state physics and electronics," *Phys. Rev. Lett.* **58**, 2059–2062 (1987).

[3] Sprik, R., van Tiggelen, B. A., and Lagendijk, A., "Optical emission in periodic dielectrics," *Eur. Phys. Lett.* **35**, 265–270 (1996).

[4] Lodahl, P., van Driel, A. F., Nikolaev, I. S., Irman, A., Overgang, K., Vanmaekelbergh, D., and Vos, W. L., "Controlling the dynamics of spontaneous emission from quantum dots by photonic crystals," *Nature* **430**, 654–657 (2004).

[5] Fujita, M., Takahashi, S., Tanaka, Y., Asano, T., and Noda, S., "Simultaneous inhibition and redistribution of spontaneous light emission in photonic crystals," *Science* **308**, 1296–1298 (2005).

[6] Rodenas, A., Zhou, G., Jaque, D., and Gu, M., "Rare-earth spontaneous emission control in three-dimensional lithium niobate photonic crystals," *Adv. Mater.* **21**, 3526–3530 (2009).

[7] Sapienza, L., Thyrrestrup, H., Stobbe, S., Garcia, P. D., Smolka, S., and Lodahl, P., "Cavity quantum electrodynamics with anderson-localized modes," *Science* **327**, 1352–1356 (2010).

[8] Jorgensen, M. R., Galusha, J. W., and Bart, M. H., "Strongly modified spontaneous emission rates in diamond-structured photonic crystals," *Phys. Rev. Lett.* **107**, 143902 (2011).

[9] Leistikow, M. D., Mosk, A. P., Yeganegi, E., Huisman, S. R., Lagendijk, A., and Vos, W. L., "Inhibited spontaneous emission of quantum dots observed in a 3d photonic band gap," *Phys. Rev. Lett.* **107**, 193903 (2011).

[10] Yoshie, T., Scherer, A., Hendrickson, J., Khitrova, G., Gibbs, H. M., Rupper, G., Ell, C., Shchekin, O. B., and Deppe, D. G., "Vacuum rabi splitting with a single quantum dot in a photonic crystal nanocavity," *Nature* **432**, 200–203 (2004).

[11] Painter, O., Lee, R. K., Scherer, A., Yariv, A., J. D. O' Brien, Dapkus, P. D., and Kim, I., "Two-dimensional photonic band-gap defect mode laser," *Science* **284**, 1819–1821 (1999).

[12] Park, H.-G., Kim, S.-H., Kwon, S.-H., Ju, Y.-G., Yang, J.-K., Baek, J.-H., Kim, S.-B., and Lee, Y.-H., "Electrically driven single-cell photonic crystal laser," *Science* **305**, 1444–1447 (2004).

[13] Altug, H., Englund, D., and Vučković, J., "Ultrafast photonic crystal nanocavity laser," *Nature Physics* **2**, 484–488 (2006).

[14] Nozaki, K., Kita, S., and Baba, T., "Room temperature continuous wave operation and controlled spontaneous emission in ultrasmall photonic crystal nanolaser," *Opt. Express* **15**, 7506–7504 (2007).

[15] van der Slot, P. J. M., Denis, T., van Dijk, M. W., Lee, J. H. H., and Boller, K.-J., "Photonic free-electron lasers," *IEEE Photon. J.* **4**, 570–573 (2012).

[16] Park, H. K., Oh, J. R., and Do, Y. R., "2d SiNx photonic crystal coated $Y_3Al_5O_{12}$:Ce^{3+} ceramic plate phosphor for high-power white light-emitting diodes," *Opt. Express* **19**, 25593–25601 (2011).

[17] Florescu, M., Lee, H., Puscasu, I., Pralle, M., Florescu, L., Ting, D. Z., and Dowling, J. P., "Improving solar cell efficiency using photonic band-gap materials," *Sol. energ. mat. sol. c.* **91**, 1599–1610 (2007).

[18] Ko, D.-H., Tumbleston, J. R., Zhang, L., Williams, S., DeSimone, J. M., Lopez, R., and Samulski, E. T., "Photonic crystal geometry for organic solar cells," *Nano Letters* **9**, 2742–2746 (2009).

[19] Johnson, S. G. and Joannopoulos, J. D., "Block-iterative frequency-domain methods for Maxwell's equations in a planewave basis," *Opt. Express* **8**, 173–190 (2001).

[20] Oskooi, A. F., Roundy, D., Ibanescu, M., Bermel, P., Joannopoulos, J. D., and Johnson, S. G., "Meep: A flexible free-software package for electromagnetic simulations by the FDTD method," *Comput. Phys. Commun.* **181**, 687–702 (2010).

[21] CST AG, *CST Microwave Studio 2011.* Bad Nauheimer Str. 19, 64289 Darmstadt, Germany.

[22] Vector Fields Software, *Concerto V7.5.* Cobham CTS Ltd., Brook Road, BH21 2BJ, Wimborne, Dorset, United Kingdom.

[23] Englund, D. and Vučković, J., "A direct analysis of photonic nanostructures," *Opt. Express* **14**, 3472–3483 (Apr 2006).

[24] Khankhoje, U. K., Kim, S.-H., Richards, B. C., Hendrickson, J., Sweet, J., Olitzky, J. D., Khitrova, G., Gibbs, H. M., and Scherer, A., "Modelling and fabrication of GaAs photonic-crystal cavities for cavity quantum electrodynamics," *Nanotechnology* **21**(6), 065202 (2010).

[25] Hecht, B., Bielefeldt, H., Inouye, Y., Pohl, D. W., and Novotny, L., "Facts and artifacts in near-field optical microscopy," *J. Appl. Phys.* **81**, 2492–2498 (1997).

[26] Carminati, R., Madrazo, A., Nieto-Vesperinas, M., and Greffet, J.-J., "Optical content and resolution of near-field optical images: influence of the operating mode," *J. Appl. Phys.* **82**, 501–509 (1997).

[27] Weston, K. D. and Buratto, S. K., "A reflection near-field scanning optical microscope technique for subwavelength resolution imaging of thin organic films," *J. Phys. Chem. B* **101**, 5684–5691 (1997).

[28] Valle, P. J., Greffet, J.-J., and Carminati, R., "Optical contrast, topographic contrast and artifacts in illumination-mode scanning near-field optical microscopy," *J. Appl. Phys.* **86**, 648–656 (1999).

[29] Labardi, M., Patane, S., and Allegrini, M., "Artifact-free near-field optical imaging by apertureless microscopy," *Appl. Phys. Lett.* **77**, 621–623 (2000).

[30] Balistreri, M. L. M., Gersen, H., Korterik, J. P., Kuipers, L., and van Hulst, N. F., "Tracking femtosecond laser pulses in space and time," *Science* **294**, 1080–1082 (2001).

[31] Bozhevolnyi, S. I., Volkov, V. S., Arentoft, J., Boltasseva, A., Sondergaard, T., and Kristensen, M., "Direct mapping of light propagation in photonic crystal waveguides," *Opt. Commun.* **212**, 51–55 (2002).

[32] Okamoto, L., Loncar, M., Yoshie, T., Scherer, A., Qiu, Y., and Gogna, P., "Near-field scanning optical microscopy of photonic crystal nanocavities," *Appl. Phys. Lett.* **82**, 1676–1678 (2003).

[33] Flück, E., van Hulst, N. F., Vos, W. L., and Kuipers, L., "Near-field optical investigation of three-dimensional photonic crystals," *Phys. Rev. E* **68**, 15601(R) (2003).

[34] Kramper, P., Agio, M., Soukoulis, C. M., Birner, A., Müller, F., Wehrspohn, R. B., Gösele, U., and Sandoghdar, V., "Highly directional emission from photonic crystal waveguides of subwavelength width," *Phys. Rev. Lett.* **92**, 113903 (2004).

[35] Tao, H.-H., Liu, R.-J., Li, Z.-Y., Feng, S., Liu, Y.-Z., Ren, C., Cheng, B.-Y., Zhang, D.-Z., Ma, H.-Q., Wu, L.-A., and Zhang, Z.-B., "Mapping of complex optical field patterns in multimode photonic crystal waveguides by near-field scanning optical microscopy," *Phys. Rev. B* **74**, 205111 (2006).

[36] Abashin, M., Tortora, P., Märki, I., Levy, U., Nakagawa, W., Vaccaro, L., Herzig, H., and Fainman, Y., "Near-field characterization of propagating optical modes in photonic crystal waveguides," *Opt. Express* **14**, 1643–1657 (2006).

[37] Lee, K. G., Kihm, H. W., Kihm, J. E., Choi, W. J., Kim, H., Ropers, C., Park, D. J., Yoon, Y. C., Choi, S. B., Woo, D. H., Kim, J., Lee, B., Park, Q. H., Lienau, C., and Kim, D. S., "Vector field microscopic imaging of light," *Nature Photonics* **1**, 53–56 (2007).

[38] Seo, M. A., Adam, A. J. L., Kang, J. H., Lee, J. W., Jeoung, S. C., Park, Q. H., Planken, P. C. M., and Kim, D. S., "Fourier-transform terahertz near-field imaging of one-dimensional slit arrays: mapping of electric-field-, magnetic-field-, and poynting vectors," *Opt. Express* **15**, 11781–11789 (Sep 2007).

[39] Vignolini, S., Intonti, F., Riboli, F., Wiersma, D. S., Balet, L., Li, L. H., Francardi, M., Gerardino, A., Fiore, A., and Gurioli, M., "Polarization-sensitive near-field investigation of photonic crystal microcavities," *Appl. Phys. Lett.* **94**, 163102 (2009).

[40] Schnell, M., Garcia-Etxarri, A., Alkorta, J., Aizpurua, J., and Hillenbrand, R., "Phase-resolved mapping of the near-field vector and polarization state in nanoscale antenna gaps," *Nano Letters* **10**, 3524–3528 (2010).

[41] Dahdah, J., Pilar-Bernal, M., Courjal, N., Ulliac, G., and Baida, F., "Near-field observations of light confinement in a two dimensional lithium niobate photonic crystal cavity," *J. Appl. Phys* **110**, 074318 (2011).

[42] Kohlgraf-Owens, D. C., Sukhov, S., and Dogariu, A., "Optical-force-induced artifacts in scanning probe microscopy," *Opt. Lett.* **36**, 4758–4760 (2011).

[43] Esslinger, M., Dorfmüller, J., Khunsin, W., Vogelgesang, R., and Kern, K., "Background-free imaging of plasmonic structures with cross-polarized apertureless scanning near-field optical microscopy," *Rev. Sci. Instrum.* **83**, 033704 (2012).

[44] Denis, T., Reijnders, B., Lee, J. H. H., van der Slot, P. J. M., Vos, W. L., and Boller, K.-J., "Method to map individual electromagnetic field components inside a photonic crystal," *Opt. Express* **20**, 22902–22913 (2012).

[45] Maier, L. C., *Field strength measurements in resonant cavities*, PhD thesis, Massachusetts Institute of Technology (1949).

[46] Maier, L. C. and Slater, J. C., "Field strength measurements in resonant cavities," *J. Appl. Phys.* **23**, 68–78 (1952).

[47] Johnson, C. C., [*Field and wave electrodynamics*], McGraw-Hill (1965).

[48] Marsh, R. A., Shapiro, M. A., Temkin, R. J., Dolgashev, V. A., Laurent, L. L., Lewandowski, J. R., Yeremian, A. D., and Tantawi, S. G., "X-band photonic band-gap accelerator structure breakdown experiment," *Phys. Rev. ST Accel. Beams* **14**, 021301 (2011).

[49] Denis, T., van der Slot, P. J. M., and Boller, K.-J., "Experimental design of a single beam photonic free-electron laser," in [*Proc. of FEL 2009*], 431–434 (2009).

[50] Guru, B. and Hiziroglu, H., [*Electromagnetc field theory and fundamentals*], PWS Pub Co (1997).

[51] Guo, H., Carmel, Y., Lou, W. R., Chen, L., Rodgers, J., Abe, D. K., Bromborsky, A., Destler, W., and Granatstein, V., "A novel highly accurate synthetic technique for determination of the dispersive characteristics in periodic slow wave circuits," *IEEE Trans. Microwave Theory Techn.* **40**, 2086–2094 (1992).

[52] Kageshima, M., Jensenius, H., Dienwiebel, M., Nakayama, Y., Tokumoto, H., Jarvis, S. P., , and Oosterkamp, T. H., "Noncontact atomic force microscopy in liquid environment with quartz tuning fork and carbon nanotube probe," *Appl. Surf. Sci.* **188**, 440–444 (2002).

[53] Frimmer, M., Chen, Y., and Koenderink, A. F., "Scanning emitter lifetime imaging microscopy for spontaneous emission control," *Phys. Rev. Lett.* **107**, 123602 (2011).